Princeton Plasma Physics Laboratory

PPPL- 4860

PPPL- 4860

FEMCAM Analysis of SULTAN Test Results for ITER Nb3SN Cable-conduit Conductors

Y. Zhai, P. Bruzzone, and C. Calzolaio

March, 2013

Prepared for the U.S. Department of Energy under Contract DE-AC02-09CH11466.

Princeton Plasma Physics Laboratory
Report Disclaimers

Full Legal Disclaimer

Trademark Disclaimer

PPPL Report Availability

Princeton Plasma Physics Laboratory:

http://www.pppl.gov/techreports.cfm

Office of Scientific and Technical Information (OSTI):

http://www.osti.gov/bridge

Related Links:

U.S. Department of Energy

Office of Scientific and Technical Information

Fusion Links

FEMCAM Analysis of SULTAN Test Results for ITER Nb_3Sn Cable-in-conduit Conductors

Yuhu Zhai[1,a], Pierluigi Bruzzone[2], Ciro Calzolaio[2]

[1]*Princeton Plasma Physics Laboratory, Princeton, NJ, USA*
[2]*EPFL-CRPP, 5232 Villigen PSI, Switzerland*

Performance degradation due to filament fracture of Nb_3Sn cable-in-conduit conductors (CICCs) is a critical issue in large-scale magnet design such as ITER which is currently being constructed in the South of France. The critical current observed in most SULTAN TF CICC samples is significantly lower than expected and the voltage-current characteristic is seen to have a much broader transition from a single strand to the CICC. Moreover, most conductors exhibit irreversible degradation due to filament fracture and a strain relaxation under electromagnetic cyclic loading. With recent success in monitoring thermal strain distribution in SULTAN tested CICCs and its evolution under cyclic loading from in situ T_c measurements, we apply FEMCAM to SULTAN tested CICCs to study Nb_3Sn strain sensitivity and irreversible performance degradation. FEMCAM is unique today for including strand filament fracture and the local current sharing effects. The model combines the thermal bending effect during cool down and the EM bending effect due to locally accumulating Lorentz force during magnet operation. In this paper, we focus on modeling of T_{cs} performance degradation based on the thermal strain relaxation recently measured at SULTAN for CICC initial and final EM load cycles. The goal is to study the transition broadening upon cyclic loading for the extreme cases seen in SULTAN tested CICCs to better quantify the observed conductor irreversible performance degradation due to filament fracture.

I. INTRODUCTION

Performance degradation of Nb_3Sn cable-in-conduit-conductors (CICCs) due to filament fracture is a critical issue in large-scale magnet design such as ITER which is currently being constructed in the South of France [1-9]. The critical current observed in tested CICC samples is significantly lower than expected and the voltage-current characteristic is seen to have a much broader transition from a single strand to a CICC cable [16-28]. The SULTAN results indicate that most conductors exhibit irreversible degradation with electromagnetic cyclic loading [25]. The irreversible part of the degradation mainly due to filament fracture may cause potential local buckling of the cable as a result of strain relaxation. It is by far the dominant cause of degradation and cannot be described by the existing scaling law.

Critical current and cable n-value representing the voltage-current characteristics are the two important parameters in measuring strand and cable performance degradation. Several numerical models attempting to capture the strand electro-mechanical [15], electro-thermal-mechanical [11] and the thermal-hydraulic-electro-magnetic (THELMA) behavior have been developed to understand CICC cable behavior. In this paper, we apply the Florida electro-mechanical cable model (FEMCAM) to SULTAN tested CICC samples to study the strain sensitivity and irreversible performance degradation as a result of filament fracture. FEMCAM combines the thermal bending effect during cool down and the electromagnetic bending effect due to locally accumulating Lorentz force during magnet operation. It is unique today among various cable models for including filament fracture and local current sharing effect observed in SULTAN tests. We focus on FEMCAM modeling of transition broadening of TF and CS samples under cyclic loading so to understand the distinction between the irreversible and reversible degradation. We demonstrated that both bending due to differential thermal contraction and that due to transverse magnetic load play important roles in the performance of Nb_3Sn strands and cables. The axial thermal compressive strain of Nb_3Sn, a critical input parameter to the model, however, cannot be physically measured in the past and the fitted data based on an extrapolation of the test results which already include all the degradation effect has to be used. Thanks to recent success in monitoring thermal strain distribution of SULTAN CICCs upon cyclic loading [22-23], we can now apply FEMCAM to study the influence of bending strain and filament current transfer with local current sharing effect on the critical current and n-value of Nb_3Sn strands and cables. The n-value is an important indicator of conductor performance drop as low n-values imply local non-uniform current transfer or associate with broken filaments [9]. The reduced strand n-value due to bending is derived from integration of filament critical current over strand core cross-section based on Ekin's assumption of low and high inter-filament resistivity limits (LRL and HRL), corresponding to full and no current transfer respectively [1]. The model results indicate that I_c degradation of strands under bending initially follows closely full inter-filament current transfer but shifts and falls between full current and no current transfer for a large bending strain. This implies that FEMCAM is self-consistent in modeling important bending effects and current transfer due to filament fracture even though we assume full inter-filament and inter-strand current transfer in a cable [17]. Different from stand critical current degradation, the strand n-value degradation under bending from FEMCAM with full current transfer and filament fracture becomes worse than that from no current transfer with filament fracture. This implies that the impact of filament fracture to the critical current degradation may be different from that to the strand n-value degradation. The effective cable n-value is derived from the power law relation following the strand electric field against critical current curve for field between 0.01-100 uV/m. The FEMCAM simulated T_{cs} and cable n-value during the first load cycle agree well with that from SULTAN measurement.

The results from FEMCAM after cyclic loading using the final thermal strain extracted from SULTAN samples show a better conductor T_{cs} and n-value than the SULTAN measurement, this may partially due to a much higher electrical field criteria used in FEMCAM for cable n-value calculation. Finally, we demonstrate that FEMCAM can be used to monitor the transition broadening of SULTAN tested CICCs as a result of progressive filament fracture and thermal strain accumulation of CICCs under cyclic loading, or thermal strain relaxation of some CICCs with improved performance after 1st load cycle as a result of local frictional micro-movement between the cable and the jacket.

II. MODEL FORMULATION

FEMCAM is formulated not based on first principles, but mainly based on simplified analytical formulations to capture all the essential physics observed from past CICC test data collected. In FEMCAM, the bending strain of a strand in a CICC is modeled based on the elastic buckling of a strand due to differential thermal contraction [8] and the multi-stage beam bending at strand crossing under locally accumulated magnetic load [12]. We assume full current transfer and the critical current density drops to zero if the filament tensile strain is beyond the strand irreversible limit.

A. *Strand Bending and Thermal Strain*

During cool down after heat treatment of a CICC, the differential thermal contraction between strands and steel jacket can create a large axial compressive strain on individual strands [8, 11]. Recent critical temperature measurement of SULTAN CICC samples during cyclic loading test, however, indicates that actual strand thermal strain distribution is much lower than the -0.65% fitted thermal strain data widely used in the past. Fig. 1 shows the thermal strain distribution extracted from in situ critical temperature measurement of SULTAN tested TFEU6 sample.

Fig. 2 presents the deflection of a wavy shaped strand in a TFEU6 CICC leg and the bending strain variation along a deformed strand due to both thermal load and the locally accumulated magnetic load. The strand axial compressive strain for the given -0.35% differential thermal contraction is smaller than the prescribed thermal mismatch because of strand waviness and the strand local bending effect.

We use the strand I_c at the peak bending strain to derive cable performance without introducing any averaging process along the strand.

The critical current reduction due to contact stress at strand crossing is implemented as the polynomial fitting of strand contact stress measurements [13].

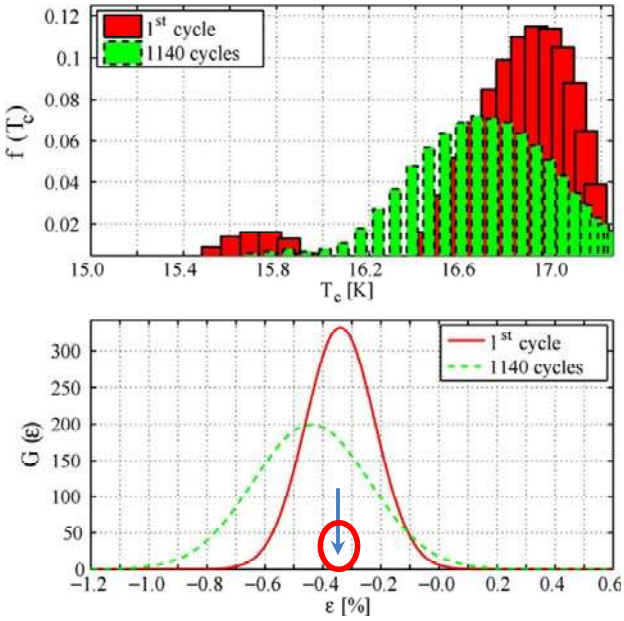

Fig. 1. Thermal strain distribution from T_c measurement (from [20]).

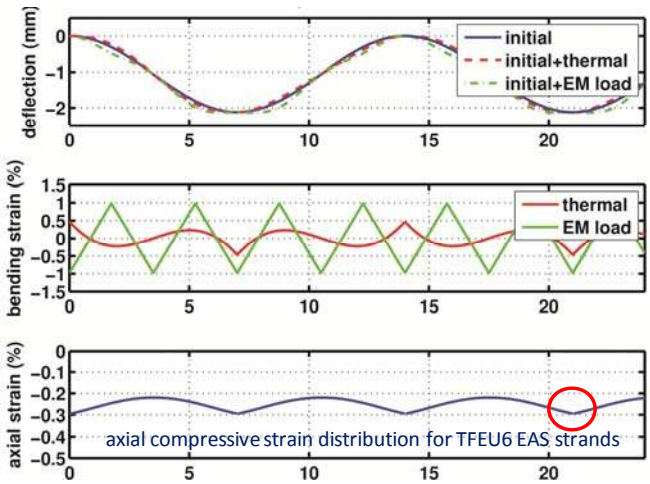

Fig. 2. FEMCAM modeled strand bending under thermal and magnetic loads

B. *Current Transfer and Filament Fracture*

The filament critical current under local bending strain is integrated over the strand core cross-section to obtain the strand critical current using Ekin's formulation and strand scaling law [1-2, 10]. Past measurements for some ITER model coil strands indicate that the reduced critical current I_c can be described by full current transfer corresponding to the low inter-filament resistivity limit [13]. Our FEMCAM analysis, however, indicates that this may only be true at a relative low strand bending strain.

Broken filaments have been known and observed in previous micrographic studies for strands under large bending [7]. We assume critical current density drops to zero in Ekin's integration if filament tensile strain is greater than the measured strand irreversible limit, despite the fact that in reality critical current density for some strands may not drop so drastically. Therefore, the filament J_c for no current transfer is the minimum between the J_c at compressive side and the J_c at the tension side.

The cable n-value is derived from slope of the electric field

versus critical current curve shown in the power law relation

$$\frac{E}{E_c} = (\frac{J}{J_c})^n , (1)$$

where E and E_c are the measured cable electric field and the electric field criteria (i.e., 0.1 uV/m).

The cable critical current reduction at each layer of strands inside a CICC is obtained by adding the I_c reduction due to total bending strain and the I_c reduction due to transverse contact force. We assume full inter-strand current transfer and add all critical current from layer to layer to obtain the average cable I_c reduction. Our assumptions of full inter-strand current transfer and the critical current drop to zero for filaments with tensile strain beyond strand irreversible limit work reasonably well in capturing critical current degradation of Nb_3Sn strands and cables.

C. Input Parameters

As an important input parameter to FEMCAM, the strand thermal compressive strain in SULTAN tested CICCs has recently been quantified from the in situ T_c measurement of the cable during initial and final load cycles. Table I listed the measured initial and final thermal strain data in various CICCs tested. The data clearly indicate thermal strain relaxation or strain accumulation under cyclic loading. The cable thermal strain change is consistent with jacket strain relaxation at the high field region. In the case of thermal strain accumulation such as that seen in TFEU6 and CSIO1, the irreversible degradation due to filament fracture increases progressively with cyclic loading, leads to potential local cable buckling with increasing cable thermal strain. In the case of progressive strain relaxation under electromagnetic cyclic loading such as seen in the TFRF3 and TFRF4 samples, frictional micro movement leads to progressive disengagement between the cable and the jacket, instead of the local buckling effect. As a result, CICCs showed an improved performance after initial cycle.

Table I. Thermal strain extracted from in situ T_c measurement

Thermal strain	TFEU6	TFRF3	TFRF4	CSIO1
Initial (%)	-0.35	-0.34	-0.36	-0.48
Final (%)	-0.44	-0.25	-0.29	-0.58

Other input parameters to the model include the strand scaling law parameters, cable void fraction, strand axial and transverse modulus, strand bending wavelength associate with cabling pattern and the twist pitch length, as well as the strand irreversible strain limit. The data are listed in Tables II and III.

III. TEST CICC SAMPLES

The SULTAN test results indicate that most CICCs show progressive performance degradation without saturation under cyclic loading [25]. The CICCs with continuous degradation in most cases such as the TFEU6/7/8 samples are dominated by irreversible filament fracture over the relatively small effect of cable settling down in the jacket during EM cyclic loading. Some CICCs such as TFRF3/4 and TFUS1/3 with solid Luvata strands show improved performance after initial cycle, mainly due to the relaxation of thermal compressive strain upon cyclic loading, which is in the range of reversible degradation as a result of cable settling down in the jacket. Similarly for the CSIO2 sample with short twist pitch, the bending is restricted by a stronger strand engagement inside the cable.

A. Continuous Performance Degradation

Fig. 3 shows the T_{cs} measurement of TFEU6 sample where progressive performance degradation with EM load cycles is clearly seen. The typical degradation behavior is similar to other TF CICCs tested and is consistent with the thermal strain accumulation observed in the initial and final cycle in situ T_c measurement. The irreversible degradation of strand inside the cable may cause potential local cable buckling as a result of incremental filament fracture upon cyclic loading. Similar behavior was observed in TFEU8 sample but with a more graduate performance drop, instead of a linear decreasing of T_{cs}.

Table II. Strand scaling parameters – Twente scaling law

CICCs	C	B^*_{c20max}	T^*_{c0max}	C_{a1}	C_{a2}	$e_{0,a}$ (%)	e_m (%)	p	q
TFEU5	9005	29.99	16.49	80.13	37.8	0.237	802	0.42	1.3
TFEU6	12447	29.88	16.06	404.87	386.71	0.139	802	0.525	1.547
TFEU8	11761	30.28	16.02	226.93	203.86	0.187	802	0.489	1.618
CSIO1	18707	33.79	16.1	44.97	0	0.28	609	0.54	2.1
CSIO2	18707	33.79	16.1	44.97	0	0.28	609	0.54	2.1
TFRF3/4	13088	32	15.44	41.16	5.84	0.27	802	0.5	1.75

Table III. FEMCAM input parameters

CICCs	Strand diam. (mm)	ε_{irr} (%)	void (%)	Bending wavelength (mm)	IxB (kN/m)
TFEU5	0.82	0.45	30.5	7	802
TFEU6	0.82	0.45	30.5	7	802
TFEU8	0.82	0.45	30.5	7	802
CSIO1-2sc	0.81	0.26	33.4	6	609
CSIO2-short	0.81	0.26	32.4	3	609
TFRF3	0.82	0.6	30.6	7	802
TFRF4	0.825	0.6	30	7	802

It may be useful to introduce a thermal strain distribution function similar to that extracted from experiment as shown in Fig. 1 or some type of filament fracture distribution observed in the past into the FEMCAM formulation to better capture uncertainty of performance degradation. It will be interesting to see the impact of the statistical distribution of FEMCAM essential input parameters to its simulation results and how the simulation correlates with measurement.

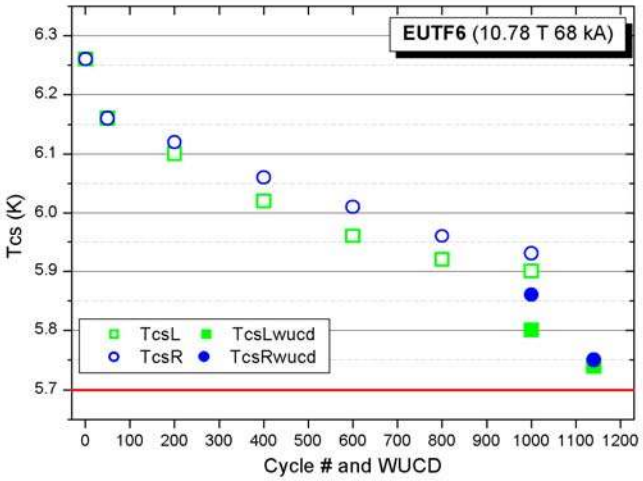

Fig.3. Tcs measurement of TFEU6 sample shows continuous performance degradation with EM load cycles [24].

B. *Improved Performance after Initial Cycle*

For CICCs with solid strands or cable with short twist pitch where the strand bending is restricted by stronger strand engagement in the cable, performance improvement after first cyclic loading mainly attributed to the frictional movement between the cable and the jacket has been observed in some CICCs such as TFRF3/4 and CSIO2 short twist pitch sample [25]. Fig. 4 shows the improved T_{cs} measurement for CSIO2 short twist pitch sample with cyclic loading.

Our past results show that the higher the excess strain, defined as total bending strain beyond the strand irreversible strain limit, the more filaments are bent to broken and thus the more additional I_c degradation occurs under cyclic load with a critical value being 0.5~0.6%. The correlation of additional degradation under cyclic load with FEMCAM results suggests that one should keep the excess strain around 0.3% or lower to minimize fatigue effects [16-17]. Past observations also indicate that short twist pitch is better when the ratio of twist pitch to sub-element diameter is below 15, where the sub-element of a cable stays intact if it was dropped several feet; however, it will fall apart if the ratio is greater than 20.

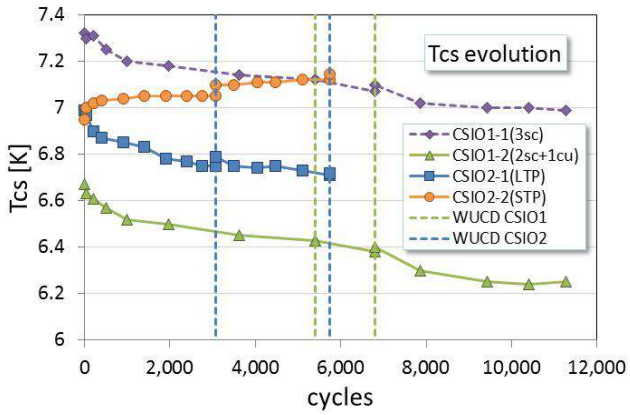

Fig.4. Tcs measurement of CSIO2 with short twist pitch shows improved performance with EM load cycles [28].

IV. FEMCAM ANALYSIS OF STRAND AND CABLE

In FEMCAM, we assume full current transfer between strands inside a cable and add all critical currents from layer to layer to get the average cable critical current reduction. The effective strand critical current is calculated using an integration procedure over strand core cross section. The effective cable critical current is calculated using a similar integration over the CICC cable cross section to account for self-field gradient and total bending strain variation over the cable cross-section under a given compressive thermal strain.

A. *Performance of Strand under Bending*

Fig. 5 and Fig. 6 represent the FEMCAM calculated J_c degradation due to bending of the EAS strand for TFEU5 and TFEU6. The degradation with filament fracture follows closely the LRL representing the full inter-filament current transfer for a less than 1% bending strain. With increasing bending strain, the degradation of HRL with filament fracture starts to deviate slightly from the curve corresponding to HRL but without filament fracture. Despite of these differences, the results imply that although we use full current transfer in FEMCAM the assumption of J_c drops to zero for filaments with strains beyond the strand irreversible limit seems reasonable in describing the influence of inter-filament current transfer to strand J_c performance degradation. Fig. 7 shows the J_c degradation due to bending of the Russian ChMP strand for TFRF3. A less compressive intrinsic strain of the Russian Bronze strand moves the strand bending closer to tensile, as a result, J_c drop has a similar behavior to the EAS strand at initial cycle even though the Russian strand has a much higher irreversible strain limit.

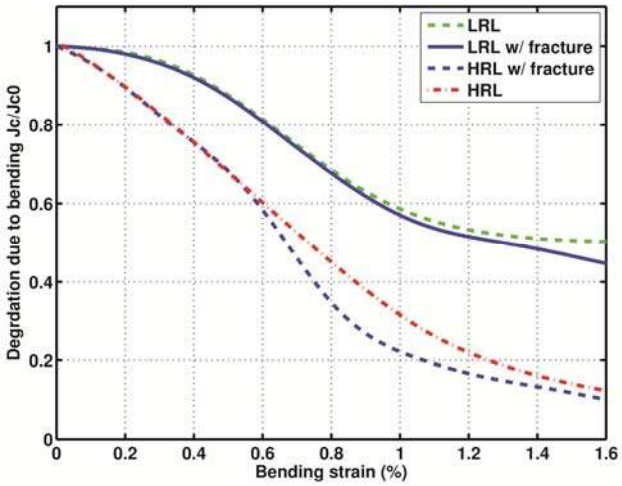

Fig.5. FEMCAM computed critical current reduction due to bending for TFEU5 EAS strand at 12 T, 4.2 K.

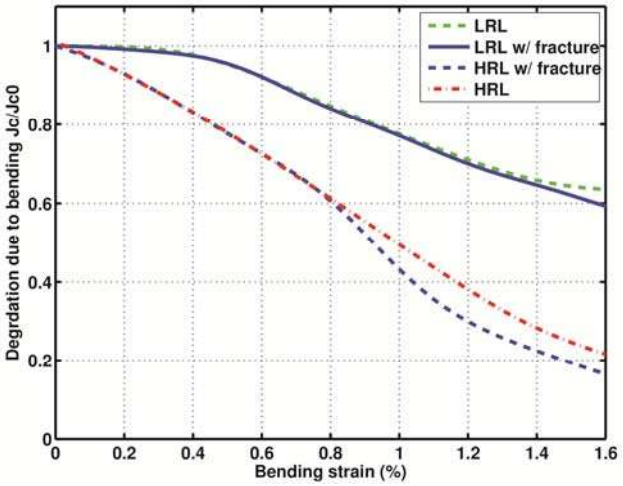

Fig.6. FEMCAM computed critical current reduction due to bending for TFEU6 EAS strand at 12 T, 4.2 K.

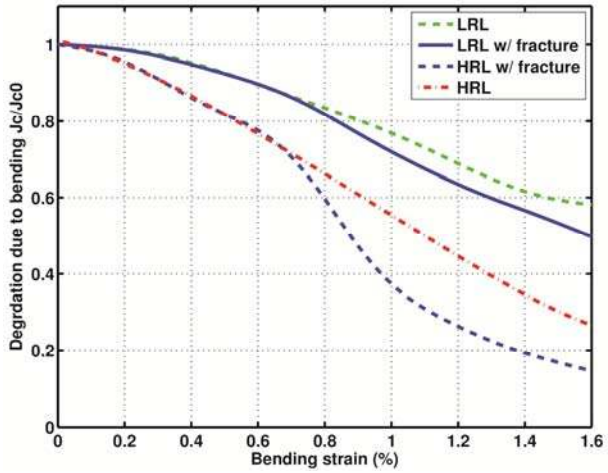

Fig.7. FEMCAM computed critical current reduction due to bending for TFRF3 ChMP Bronze strand at 12 T, 4.2 K.

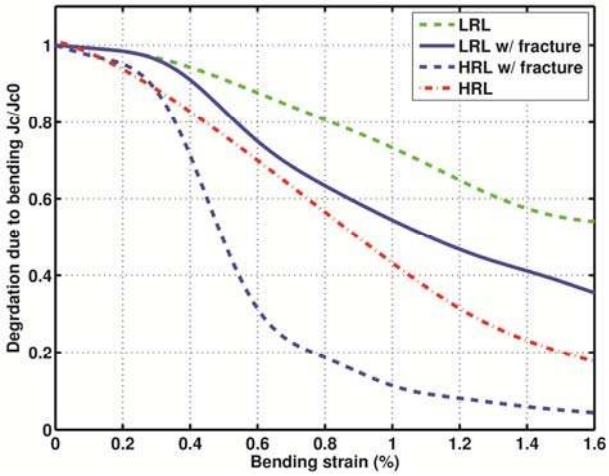

Fig.8. FEMCAM computed critical current reduction due to bending for CSIO1 OST strand at 12 T, 4.2 K.

Impact of irreversible strain limit is clearly seen in Fig. 8, where FEMCAM calculated J_c degradation due to bending of the OST strand for the CSIO1 sample is shown. Strands with a more compressive intrinsic strain show less initial impact from filament fracture, but the irreversible damage may increase progressively with cyclic loading due to locally accumulated thermal compressive strain, as a result of cable local buckling (TFEU6 and TFEU8), see later sections for more details.

It is not clear if the bending behavior of a particular strand will follow the full current transfer assumption with filament fracture or no current transfer with filament fracture. Previous results indicate that initially the strand bending behavior seems to following closely the full current transfer assumption but will gradually shift to the no current transfer behavior with increased strand bending [13,17]. This is directly related to recent statistical study on the filament fracture distribution in ITER strands [20-21]. For the case of TF CICC samples, it will be useful to see direct measurement of progressive increment of filament fracture with cyclic loading on the TFEU6&8 and compare that with the same measurement for the TFRF3&4. We expect to see a significantly less filament damage in the TFRF samples. Measurement and direct comparison of cable modulus with jacket modulus will also be very useful to validate the thermal strain relaxation between cable and jacket with cyclic loading as a result of cable and jacket frictional movement. We expect to see a stiffer TFRF cable (may be stiffer than its jacket modulus) than the TFEU cable.

A simple electrical model originally proposed by Mitchell [11] is implemented with assumptions 1) At very low electric field (i.e., 0.01 uV/m), current flow in filament is limited by lowest superconducting transport current and there is no inter-filament current transfer 2) At very high electric field (i.e., 100 uV/m), critical current is un-degraded superconducting transport current and full inter-filament current transfer is allowed. Fig. 9 presents simulated strand n-value degradation under bending strain for both full and no current transfer cases. For a small bending strain (<0.4%), we expect no n-value degradation of the strand. With an increase of the bending, n-value starts to degrade for no current transfer case first and the full current transfer case has less n-value degradation that the no current transfer case.

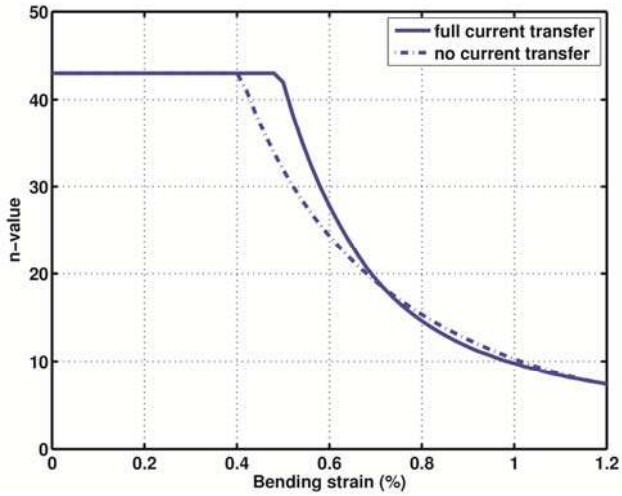

Fig.9. FEMCAM computed n-value of TFEU5-EAS strand under bending at 12 T, 4.2 K.

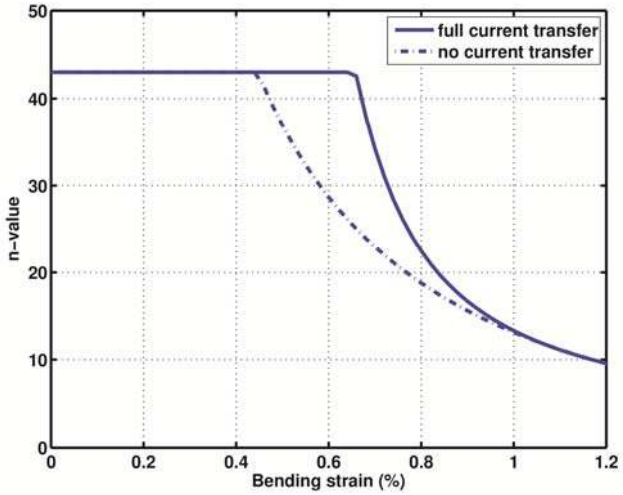

Fig.10. FEMCAM computed n-value of TFEU6-EAS strand under bending at 12 T, 4.2 K.

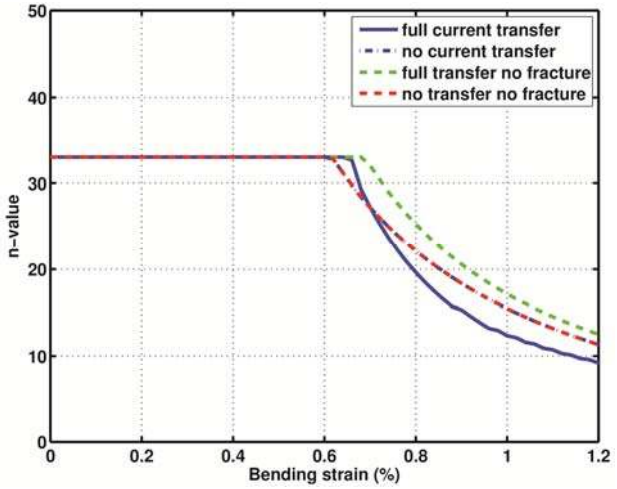

Fig.11. FEMCAM computed n-value of TFRF3 Russian strand under bending at 12 T, 4.2 K.

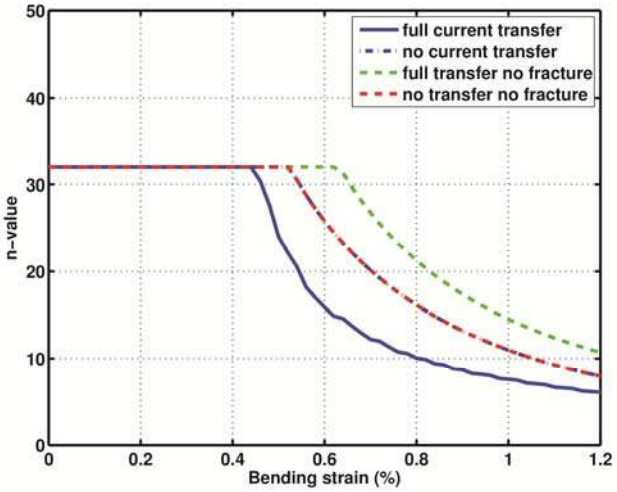

Fig.12. FEMCAM computed n-value degradation of CSIO1-2sc OST strand.

Fig. 10 presents the simulated n-value degradation for the TFEU6-EAS strand. The difference between EAS strands used in TFEU5 and TFEU6 samples is not so clear but it appears that n-value of the TFEU6-EAS strand is more sensitive to local current transfer for strand under transverse bending. The n-value degradation from FEMCAM simulation for both strands for the case of current transfer with filament fracture is very close to the case of current transfer without filament fracture effect. The irreversible strain limit used for both strands is 0.45%. Fig. 11 presents the FEMCAM computed n-value degradation for the TFRF3 Russian bronze route strand. Fig. 12 presents the same simulation result for the CSIO1-2sc OST strand. The results indicate that filament fracture impacts local current sharing more in OST strand that that in the EAS and Russian strands due to a smaller strand irreversible strain limit of the OST internal-tin strand.

The results of n-value degradation also imply that for both bronze route and internal tin strands, the strand n-value degradation may become worse for full current transfer with filament damage than that from the no inter-filament current transfer. This is different from the J_c degradation shown in Figs. 5-8 where full current transfer with filament damage always give better or less J_c degradation than that from the no current transfer with filament fracture. As a result, this may imply that filament fracture and local current sharing will impact transition broadening of strand under bending differently from its impact to the critical current degradation.

The strand critical current at high axial compressive strain is much lower and critical current drops faster with increasing bending strain for the case of no current transfer. The results imply that bending creates filament current transfer and may cause filament fracture that leads to strand performance degradation in the form of local buckling and thermal strain relaxation. A small bending strain may have minor impact to strand n-value performance, with increased bending strain, however, more and more filaments are broken and this causes transition broadening to the strand and thus to the cable.

B. 1st Cycle Performance of CICCs

The cable n-value is obtained from the slope of the log (E) versus log (J) plot as described by the empirical power law relation in Eq. (1) and the formulation was described elsewhere [17]. Table IV listed the comparison of SULTAN measured and the FEMCAM calculated cable initial current sharing temperature and n-value. Table IV also listed I_c degradation due to transverse bending and the ratio between operating current and cable critical current at 1st cycle. The results from FEMCAM simulation in general very similar and agree well with SULTAN measurements. The larger predicted degradation in CSIO1 sample is partially due to slightly larger void fraction in the CS samples. The simulated cable initial n-value is also consistent with SULTAN measurement. The FEMCAM predicts higher T_{cs} than measurement for TF CICC but lower than measured T_{cs} for the CS CICCs.

Table IV. FEMCAM predicted cable T_{cs} and n-values

CICCs	I_c deg.	Initial T_{cs} (K)		Cable n-value		I_{op}/I_c
TFEU5	16.5%	6.35*	6.33	11.9	12.5	65%
TFEU6	14.9%	6.26	6.77	13	15.7	55%
TFEU8	17.2%	6.13/6.27	6.4	15	15.1	61%
TFRF3	12.2%	6.15/6.54	6.74	14.3	14.9	54%
TFRF4	9.6%	5.98/5.92	6.46	9.9/12	13.4	58%
CSIO1	22.8%	6.67	5.94	15.9	8.7	66%
CSIO2	14.7%	6.95	6.29	14	10.9	60%

C. *Performance Evolution under Cyclic Loading*

SULTAN test results indicate that monitoring of transition broadening due to filament fracture from superconducting to normal state upon cyclic loading is the key to quantify the conductor performance degradation. To this end, we apply the thermal strain measurement and its evolution at the 1st cycle and the 1001 cycle to FEMCAM to study the impact of strain relaxation. The result of this study can be used to correlate with CICC T_{cs} measurement under cyclic loading. Fig. 13 presents the FEMCAM calculated T_{cs} performance evolution under the electromagnetic cyclic loading for the TFEU6 and TFEU8 samples. The results show a very similar trend of T_{cs} drop to that from the measurement seen in Fig. 3 and Fig. 14, where a linear strain relaxation for TFEU6 sample and a more gradual strain relaxation in TFEU8 sample are observed. In FEMCAM, 1st cyclic loading with 0.03% strain relaxation and ~0.01% relaxation every other 100 cycles were applied.

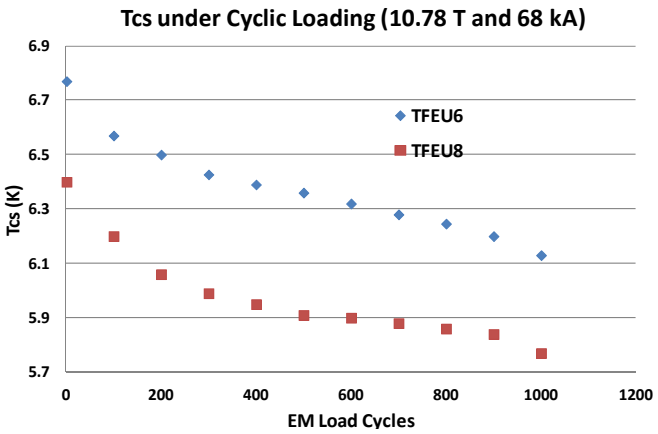

Fig.13. FEMCAM simulated Tcs degradation evolution under cyclic loading for the TFEU6 and TFEU8 samples.

Fig. 15 presents FEMCAM simulated T_{cs} evolution of TFRF3 sample where a performance improvement is clearly seen. This is different from the measurement shown in Fig. 3 and Fig. 14, where a progressive degradation is observed. The improved performance is mainly due to a local thermal strain relaxation as a result of frictional micro-movement between the cable and jacket under EM cyclic loading. In this case, it is expected that the cable may have a larger stiffness than the jacket, causing the sliding between cable and jacket, which is essentially a reversible process different from a progressive increase of irreversible filament fracture seen in TFEU6 and TFEU8 samples.

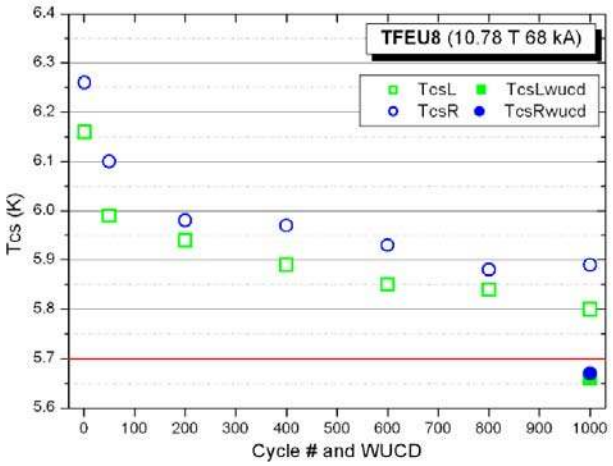

Fig.14. Tcs measurement of TFEU8 sample shows continuous performance degradation with EM load cycles [25].

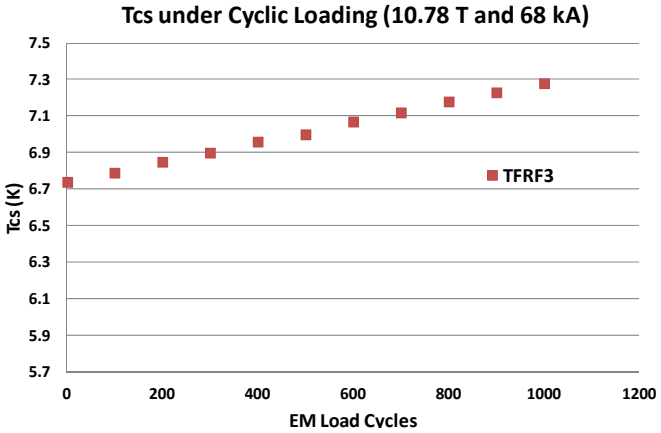

Fig.15. FEMCAM simulated Tcs evolution of TFRF3 sample shows performance improvement with EM load cycles.

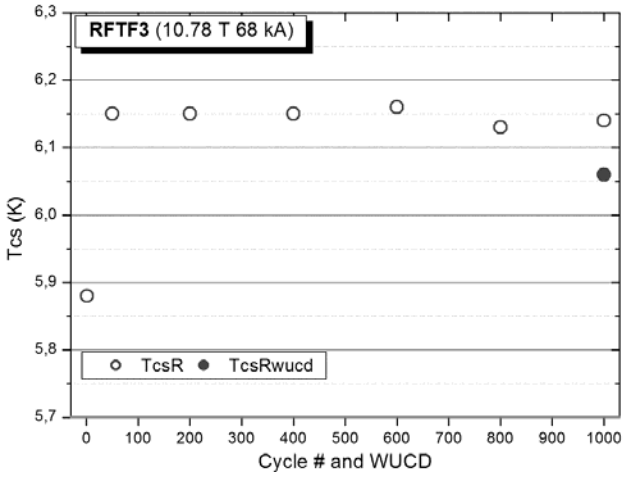

Fig.16. Tcs measurement of TFRF3 sample shows slightly performance improvement with EM load cycles [26].

Fig. 16 presents the evolution of T_{cs} measurement of the TFRF3 sample. Fig. 17 presents the applied thermal strain relaxation in FEMCAM for the simulation of performance evolution under cyclic loading for the above CICCs tested.

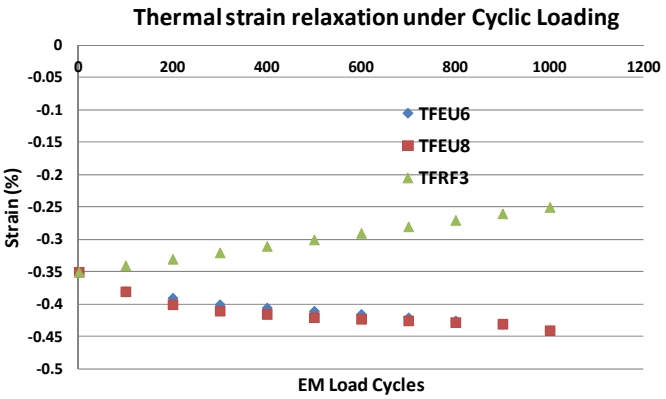

Fig.17. Thermal strain relaxation applied in FEMCAM to simulate performance evolution with cyclic loading for the TF CICCs.

Table V. FEMCAM predicted cable T_{cs} and n-values

CICCs	I_c deg.	Final T_{cs} (K)		Cable n-value		I_{op}/I_c
	FEMCAM	SULTAN	FEMCAM	SULTAN	FEMCAM	FEMCAM
TFEU5	17.7%	6.24/5.98	5.31	n/a	9.2	82%
TFEU6	15.6%	5.9	6.13	9.2/10.1	12.3	64%
TFEU8	15.4%	5.8/5.89	5.77	6.13/8.3	11.8	69%
TFRF3	12%	6.15	6.89	8.7	16.1	52%
TFRF4	9.1%	6.22/6.12	6.9	7.5/9.5	15.9	51%
CSIO1	21%	6.25	5.53	11	8.0	74%
CSIO2	15.3%	7.14	7.04	12/12.4	14.3	49%

Table V listed the measured and FEMCAM simulated T_{cs} and cable n-value after 1000 EM load cycles. The n-value of a single strand is usually measured at 4.2 K and 12 T of a typical 20-30 for internal tin Nb_3Sn strands and 30-50 for bronze route processed strands. For strands we have studied, the FEMCAM predicted cable n-values agree better in general with measurements for the 1st cycle performance as shown in Table IV, but FEMCAM simulation gives higher than the measured n-values after cyclic loading as shown in Table V. This discrepancy could be partially due to the fact that in simulation higher electric field criteria of 20-100 uV/m (assuming full current transfer with filament fracture) were used for the cable n-value calculation. The results can become sensitive to the FEMCAM assumptions of which electric field criteria is used in the simulation. Considering the simplifying assumptions and approximations involved in FEMCAM formulation, the results are still reasonably encouraging. The results indicate that FEMCAM as an effective tool can be very useful for data processing of SULTAN results and eventually a systematic study using FEMCAM could lead to a better understanding of CICC performance degradation. FEMCAM study of local current sharing effect due to filament fracture and its evolution with cyclic loading will also validate our speculations from experimental observations on the distinction of irreversible and reversible degradation behavior.

Fig. 18 and Fig. 19 present the FEMCAM simulated electric field against T_{cs} transition for the TFEU6 and TFRF3 samples for the 1st load cycle and after 1000 cycles respectively. Fig. 20 presents the FEMCAM simulated E-T transition for the 1st and after 5k EM load cycles for the CSIO1-2sc samples. The results are extracted from cable n-value calculation with the assumption that no current transfer for an electric field below 0.01 uV/m and full current transfer at the electric field of 100 uV/m. The results are still preliminary and correlation with experiments will be studied in the following work. The results, however, provide a proof of concept that FEMCAM can be used for modeling the superconducting to normal transition region for monitoring cable n-value degradation and transition broadening, which is the key to better quantify the conductor performance degradation.

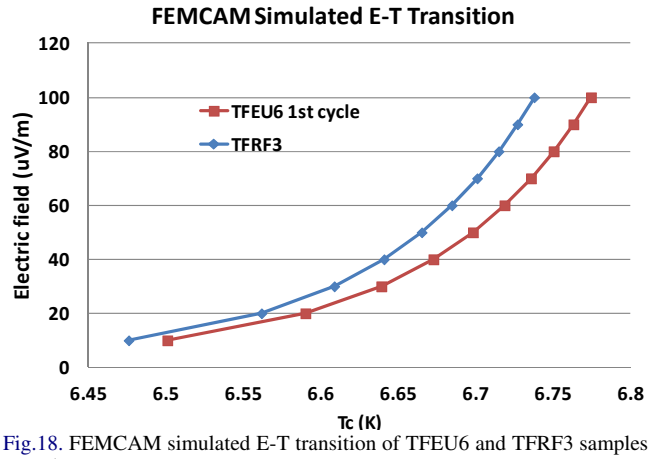

Fig.18. FEMCAM simulated E-T transition of TFEU6 and TFRF3 samples for the 1st cycle.

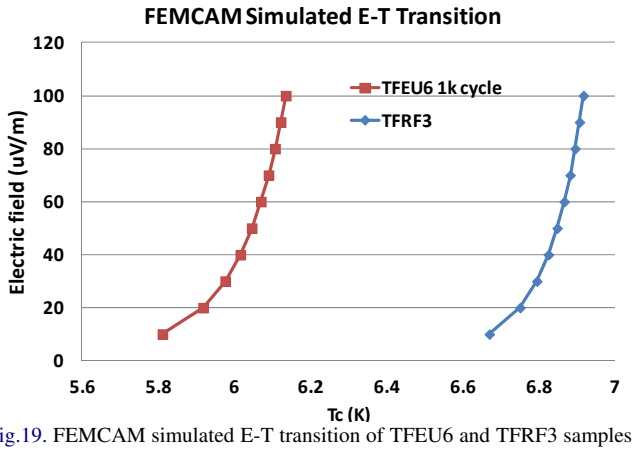

Fig.19. FEMCAM simulated E-T transition of TFEU6 and TFRF3 samples for the 1001 EM load cycle.

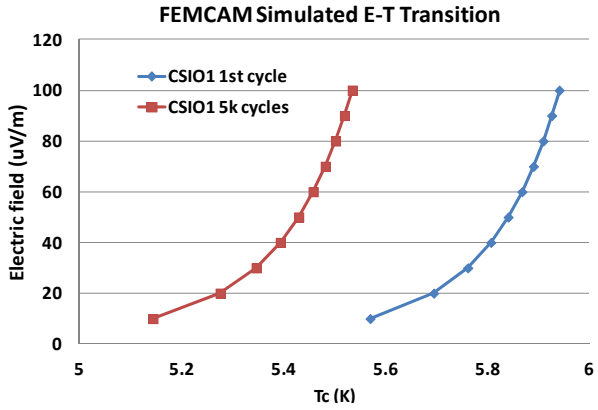

Fig.20. FEMCAM simulated E-T transition of CSIO1-2sc sample for the 1st and after 5k EM load cycles.

V. CONCLUSION AND DISCUSSION

Most CICC samples tested in SULTAN show progressive performance degradation with cyclic EM loading. The critical current observed in test samples is significantly lower than expected and the voltage-current characteristic is seen to have a much broader transition from a single strand to a CICC cable. The test results indicate that most conductors exhibit irreversible degradation with electromagnetic load cycling. The irreversible part of degradation is due to filament fracture and local strain accumulation. It is by far the dominant cause of degradation and cannot be described by the existing scaling law.

FEMCAM is a useful cable modeling tool that combines the thermal bending effect during cool down and the EM bending effect due to the locally accumulating Lorentz force during magnet operation. The model is unique today among various existing electrical and mechanical cable models for including filament fracture and local current sharing effect observed in SULTAN tests. We apply FEMCAM to study SULTAN test results to understand the strain sensitivity and irreversible performance degradation of ITER CICCs. The model predicts I_c degradation of strand under bending initially follows curve of full inter-filament current transfer but deviates and falls between full current and no current transfer for large bending strain. The reduction of effective strand core cross-section as a result of progressive filament fracture under large bending needs to be validated by experiment. The simulated strand n-value degradation for full current transfer with filament fracture becomes worse than that for no current transfer. This is not consistent with I_c degradation of strand under bending, where full current transfer case with filament fracture is always better than no current transfer case, but implies that filament fracture impacts strand local current sharing and transition broadening differently as it impacts the critical current degradation.

We also apply FEMCAM to model transition broadening of CICCs under cyclic loading so to understand the distinction between irreversible and reversible degradation. It is still not clear how to correlate the observed progressive increment of filament fracture in a cabled strand with cyclic loading. The development of a local transition region from full current transfer to no current transfer with increased bending still needs to be understood. With the SULTAN experimental data, we hope to be able to perform a systematic FEMCAM analysis soon for a better prediction of CICC performance.

ACKNOWLEDGMENT

This work is supported by US DOE contract numbers DE-AC02-09CH11466. The authors thank Phil Heitzenroeder at Princeton Plasma Physics Laboratory for his considerable effort in supporting this work.

REFERENCES

[1] J.W. Ekin, "Strain scaling law and the prediction of uniaxial and bending strain effects in multifilamentary superconductors," *Proc. Topical Conf. on A-15 Supercond.*, Plenum, New York, 1980.

[2] J.W. Ekin, "Effect of transverse compressive stress on the critical current and upper critical field of Nb_3Sn," *J. Appl. Phys*., vol.62, pp.4829-4834, 1987.

[3] L.T. Summers et al, "A model for the prediction of Nb_3Sn critical current as a function of field, temterature and radiation damage," *IEEE Trans. on Magnetics*, vol.27, pp.2041-2044, 1991.

[4] N. Mitchell, "Steady state analysis of non-uniform current distributions in cable-in-conduit conductors and comparison with experimental data," *Cryogenics*, vol. 40, pp. 99–116, 2000.

[5] P. Bruzzone, A. M. Fuchs, B. Stepanov, and G. Vecsey, "Performance evolution of Nb_3Sn cable-in-conduit conductors under cyclic load," *IEEE Appl. Supercond.*, vol. 12, pp. 516–519, 2002.

[6] P. Bruzzone, R. Wesche, and B. Stepanov, "The voltage/current characteristic (n index) of the cable-in-conduit conductors for fusion," *IEEE Trans. Appl. Supercond.*, vol. 13, pp. 1452–1455, 2003.

[7] M.C. Jewell, P.J. Lee, and D.C. Larbalestier, "The influence of Nb_3Sn strand geometry on filament breakage under bend strain as revealed by metallography", *Supercond. Sci. Technol.*, vol. 16, pp. 1005–1011, 2003.

[8] N. Mitchell, "Mechanical and magnetic load effects in Nb_3Sn cable-in-conduit conductors," *Cryogenics*, vol. 43, pp. 255–270, 2003.

[9] P. Bruzzone, "The index n of the voltage-current curve, in the characterization and specification of technical superconductors", *Physica C: Supercond*., vol. 401, pp.7-14, 2004.

[10] L. Bottura and B. Bordini, "$Jc(B,T,e)$ parameterization for the ITER Nb3Sn production", *IEEE Trans. Appl. Supercond.*, vol. 19, pp. 1521–1524, 2009.

[11] N. Mitchell, "Operating strain effects in Nb_3Sn cable-in-conduit conductors," *Supercond. Sci. Technol.*, vol. 18, pp. 396–404, 2005.

[12] A. Nijhuis and Y. Ilyin, "Transverse load optimization in Nb_3Sn CICC design; influence of cabling, void fraction and strand stiffness", *Supercond. Sci. Technol.*, vol.19, pp. 945–962, 2006.

[13] A. Nijhuis et al, "Critical current and strand stiffness of three types of Nb_3Sn strand subjected to spatial periodic bending", *Supercond. Sci. Technol.*, vol.19, pp. 1136–1145, 2006.

[14] P. Bruzzone et al, "Transverse load degradation in Nb_3Sn cable-in-conduit conductors with different cable pattern," *Adv. Cryog. Eng.*, vol. 52, pp. 558–565, 2006.

[15] N. Mitchell, "Assessment of conductor degradation in the ITER CS insert coil and implications for the ITER conductors," *Supercond. Sci. Technol.*, vol. 20, pp. 25–34, 2007.

[16] Y. Zhai, M.D. Bird, "Florida electro-mechanical cable model of Nb_3Sn CICCs for high-field magnet design", *Supercond. Sci. Technol.*, vol. 21, 115010, 2008.

[17] Y. Zhai, "Electro-mechanical modeling of Nb3Sn CICC performance degradation due to strand bending and inter-filament current transfer", Cryogenics, v50, 149-157, 2010.

[18] A. Nijhuis, "Performance of ITER (EU-TFPRO-2) Nb_3Sn strands under spatial periodic bending, axial strain and contact stress," *IEEE Appl. Supercond.*, vol. 18, pp. 1059–1062, 2008.

[19] A. Nijhuis, "A solution for transverse load degradation in ITER Nb_3Sn CICCs: verification of cabling effect on Lorentz force response", *Supercond. Sci. Technol.*, vol.21, 054011, 2008.

[20] A. Nijhuis et al, "Systematic study on filament fracture distribution in ITER Nb_3Sn strands", *IEEE Trans. Appl. Supercond.*, vol. 19, n3, 2009.

[21] D. Uglietti, "Statistical analysis of current-sharing temperature evolution in Nb3Sn CICC for ITER", *IEEE Trans. Appl. Supercond.*, vol.22, 4802204, 2012.

[22] C. Calzolaio, P. Bruzzone and D. Uglietti, "Measurement of Tc distribution in Nb_3Sn CICC", *Supercond. Sci. Technol.*, 054007, 2012.

[23] C. Calzolaio, P. Bruzzone and B. Stepanov, "Monitoring of the thermal strain distribution in CICCs during the cyclic loading tests in SULTAN", *IEEE Trans. Appl. Supercond.*, vol. 23, 4200404, 2013.

[24] M. Breschi et al, "Results of the TF conductor performance qualification samples for the ITER project", *Supercond. Sci. Technol.*, 095004, 2012.

[25] P. Bruzzone et al, "Test results of ITER conductors in the SULTAN Facility", *24th IAEA Fusion Energy Conference*, 2012.

[26] V.I. Tronza et al, "Testing of RF 100m TF qualification conductor in the SULTAN test facility", *IEEE Trans. Appl. Supercond.*, to appear, 2013.

[27] S. March et al, "Results of the TFEU6 sample tested in SULTAN", *IEEE Trans. Appl. Supercond.*, vol. 23, 4200204, 2013.

[28] A. Nijhuis and G. Rolando, "Summary and analysis of CSIO1 and 2 results", Intermediate report UT-IO-2012-2.2, September, 2012.

The Princeton Plasma Physics Laboratory is operated
by Princeton University under contract
with the U.S. Department of Energy.

Information Services
Princeton Plasma Physics Laboratory
P.O. Box 451
Princeton, NJ 08543

Phone: 609-243-2245
Fax: 609-243-2751
e-mail: pppl_info@pppl.gov
Internet Address: http://www.pppl.gov